We are IntechOpen, the world's leading publisher of Open Access books Built by scientists, for scientists

4,800
Open access books available

122,000
International authors and editors

135M
Downloads

Our authors are among the

154
Countries delivered to

TOP 1%
most cited scientists

12.2%
Contributors from top 500 universities

CLARIVATE ANALYTICS BOOK CITATION INDEX INDEXED

WEB OF SCIENCE™

Selection of our books indexed in the Book Citation Index in Web of Science™ Core Collection (BKCI)

Interested in publishing with us?
Contact book.department@intechopen.com

Numbers displayed above are based on latest data collected.
For more information visit www.intechopen.com

5

Hydrogen Storage Properties of Hydrogenated Graphite and Lithium Hydride Nanocomposite

Takayuki Ichikawa, Hiroki Miyaoka and Yoshitsugu Kojima
Hiroshima University,
Japan

1. Introduction

Recently, hydrogen storage and transportation are being studied all over the world as the key technology to establish clean and renewable energy systems for a sustainable society. In the case of an on−board application for a vehicle, hydrogen should be stored in a compact, light, safe, and reasonable vessel. Hydrogen storage materials can safely store higher density of hydrogen compared to the gaseous and liquid hydrogen storage systems. Therefore, the systems using hydrogen storage materials are considered as the most suitable technique (Akiba, 1999, Grochala & Edwards, 2004, Sandrock, 1999, Schlapbach & Züttel, 2001, Züttel, 2007). Particularly, much attention has been paid to materials based on the light elements because these materials are expected to realize high gravimetric and volumetric densities of hydrogen (Orimo & Nakamori et al., 2007, Schüth & Bogdanović et al., 2004, Züttel, 2004).
Carbon is one of the attractive light elements because of abundant resource and low cost. Therefore, a lot of carbon based materials have been investigated as a hydrogen storage material since Dillon *et al*. reported on single−walled carbon nano−tubes in 1997 (Dillon & Jones et al., 1997). Among the carbon based materials, the hydrogenated nano−structural graphite ($C^{nano}H_x$) can stably store large amount of hydrogen. The hydrogen ab/desorption properties of $C^{nano}H_x$ have been investigated so far (Chen et al., 2003, Ichikawa et al., 2004, Majer et al., 2003, Miyaoka et al., 2010, Orimo et al., 1999, Orimo et al., 2001, Stanik et al., 2005). $C^{nano}H_x$ is synthesized from graphite by ball−milling method under hydrogen atmosphere. With respect to the hydrogen absorption site in this product, the hydrogen atoms are chemisorbed as the stable C−H bonds at the graphene edges and defects induced by ball−milling (Fukunaga & Itoh et al., 2004, Itoh & Miyahara et al., 2003, Ogita & Yamamoto et al., 2004, Smith & Miyaoka et al., 2009). On the other hand, this product needs a high temperature of more than 700 °C to release the hydrogen, and desorbs a considerable amount of hydrocarbons, such as methane (CH_4) and ethane (C_2H_6), together with hydrogen. Furthermore, it is quite difficult to recharge this product with hydrogen under moderate conditions of pressure and temperature for the on−board application. In order to improve the hydrogen absorption and desorption properties of $C^{nano}H_x$, Ichikawa *et al*. have paid attention to the chemical reaction between NH_3 and LiH, which is one of the elementary reactions in the Li−N−H system (Ichikawa & Hanada et al., 2004). This reaction proceeds even at room temperature and the hydrogen is released, indicating that the stable ionic crystal of LiH is

destabilized by reacting with polar molecule ammonia (NH_3) to form lithium amide ($LiNH_2$). On the analogy of this reaction, a hydrogen storage system using a reaction between $C^{nano}H_x$ and LiH has been designed, where the C−H groups in $C^{nano}H_x$ are polarized (similar to NH_3) as is clear from the existence of the IR active modes corresponding to the C−H bonding (Ogita et al., 2004). In fact, it was demonstrated that the hydrogen absorption and desorption properties of $C^{nano}H_x$ is improved by synthesizing the nano-composites with LiH (Ichikawa & Fujii et al., 2005, Ichikawa & Isobe et al., 2005). The Li−C−H system would be categorized as a new hydrogen storage system because the hydrogen absorption and desorption reactions would be induced by a characteristic interaction between the polarized C−H groups in nano−structural graphite and LiH, which is not reported so far. Therefore, the hydrogen absorption and desorption reactions are quite different from the conventional hydrogen storage systems, indicating that an understanding of the hydrogen ab/desorption properties of the systems could lead to design a new hydrogen storage system with further high performance.

In this chapter, the details of hydrogen absorption and desorption mechanism on the $C^{nano}H_x$−LiH composite is discussed on the basis of the experimental results obtained by various kinds of analyses. In addition, the similar systems composed of $C^{nano}H_x$ and other alkali (−earth) metal hydrides are also introduced.

2. Experimental details

2.1 Sample preparation

The hydrogenated nano−structural graphite ($C^{nano}H_x$ or $C^{nano}D_x$) was synthesized from high purity graphite powder by the vibrating ball−mill apparatuses. Graphite of 300 mg and 20 ZrO_2 balls with 8 mm in diameter were put into a milling vessel made of Cr steel. Then, the ball−milling was performed under 1.0 MPa H_2 or D_2 pressure at room temperature for 80 h. In order to synthesize the composites, $C^{nano}H_x$ (or $C^{nano}D_x$) and *M*H (*M*=Li, Na, Mg, and Ca) were mechanically milled for 2 h under a 1.0 MPa H_2 atmosphere at room temperature by using a rotating ball−mill apparatus. The molar ratio of $C^{nano}H_x$ and LiH was chosen to be 2:1 as a suitable composition from previous studies (Ichikawa et al., 2005). The dehydrogenating and rehydrogenating treatments for the composites were performed at 350 °C for 8 h under high vacuum condition and 3.0 MPa H_2 pressure in a reactor made of steel, respectively. The details of sample preparation are shown in the previous articles (Ichikawa et al., 2005, Miyaoka et al., 2007, Miyaoka et al., 2009, Miyaoka et al., 2008).

2.2 Experimental techniques

Thermal gas desorption properties of the composites were examined by a thermal desorption mass spectroscopy (TDMS) connected to thermogravimetry (TG) and differential scanning calorimetry (DSC). Phase identification for the composites at each stage was carried out by powder X−ray diffraction (XRD) measurement (CuKα radiation). The neutron diffraction measurements for the deutrated composites ($C^{nano}D_x$−LiD) were carried out using high intensity total scattering spectrometer (HIT−II) at the high energy accelerator research organization (KEK, Tsukuba, Japan). The remaining gases in the reactor used to rehydrogenate the composites by the heat treatment were identified by gas chromatography (GC). The details of above analyses are described in the articles reported before (Fukunaga et al., 2004, Itoh et al., 2003, Miyaoka et al., 2007, Miyaoka et al., 2009, Miyaoka et al., 2008).

3. Results and discussion

3.1 Hydrogen absorption and desorption mechanism of the $C^{nano}H_xLiH$ composite

Fig. 1 shows the TDMS and TG profiles of the composites after synthesizing and after each cycle of hydrogen absorption/desorption up to 5 times, where mass number 2, 16, and 28 are assigned to H_2, CH_4, and C_2H_6, respectively (Ichikawa et al., 2005, Miyaoka et al., 2009). In the TDMS profile of the as−synthesized composite shown in Fig. 1, the intensities of CH_4 and C_2H_6 are enlarged to ten times. From the result, it is found that this composite desorbs the hydrogen around 350°C with small amount of hydrocarbon desorption. The hydrogen desorption peak temperature is lower than the decomposition temperatures of $C^{nano}H_x$ and LiH themselves. The TG profile of the as−synthesized composite (dash and dot line in Fig. 1) reveals a weight loss of about 10.0 mass % during heating up to 500°C.

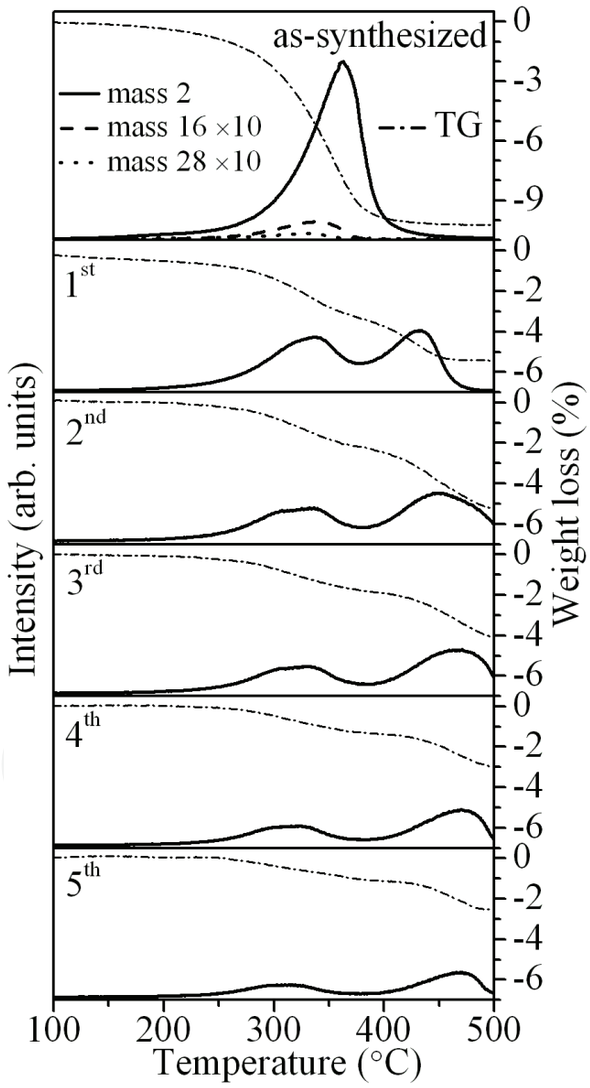

Fig. 1. TDMS and TG profiles (dash and dot line) of the $C^{nano}H_x$-LiH composites after synthesizing and rehydrogenation of 5 times.

This weight loss is mostly due to hydrogen gas, but includes a small amount of hydrocarbon desorption. After the dehydrogenation and rehydrogenation cycles, the hydrogen desorption profile of the composites reveal a two−peak structure, where these peaks correspond to hydrogen desorption are located around 350 and 450°C. These hydrogen desorption temperatures are still lower than the decomposition temperature of each component, suggesting that the hydrogen desorption of cycled composites could take place by the interaction between the polarized C−H groups and LiH. It should be noticed that only hydrogen is desorbed from the rehydrogenated composites without any hydrocarbons emission, suggesting that hydrogen absorption state of the hydrogen recharged composite is slightly different from that of the as−synthesized composite. The hydrogen desorption peak around 450°C in the TDMS profile may be caused by the slow reaction kinetics because this peak almost disappeared in the TDMS after the 2nd dehydrogenation at 350°C. The 1st and 2nd rehydrogenated composites can desorb 5.0 mass % of hydrogen as shown in their TG profiles. However, the hydrogen desorption amount gradually decreases with the hydrogen ab/desorption cycles after the 3rd rehydrogenation although the shape of the hydrogen desorption profiles are almost unchanged.

The structural change with the hydrogenation and dehydrogenation cycles was examined by XRD measurements. The XRD profiles of the composite after synthesis and after each dehydrogenation and rehydrogenation treatment are shown in Fig. 2 (Miyaoka et al., 2009). As a reference, the XRD profiles of LiH (PDF #65−2897) and Li_2C_2 (PDF #21−0484) in the database are shown.

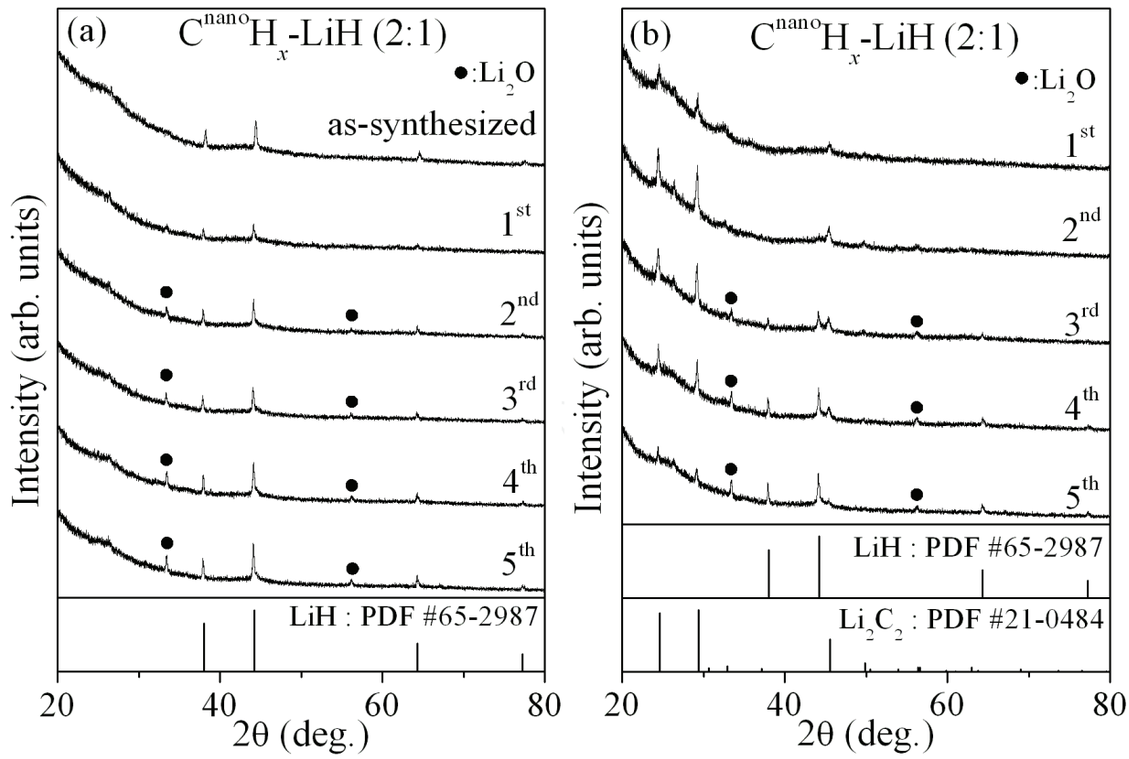

Fig. 2. XRD patterns of (a) the hydrogenated and (b) the dehydrogenated $C^{nano}H_x$-LiH composites at room temperature after each dehydrogenating and rehydrogenating treatments.

In the XRD pattern of the as−synthesized composite in Fig. 2 (a), diffraction peaks corresponding to a LiH phase are observed, and no other peaks related to carbon appear due to the nano−structural feature. After the 1st dehydrogenation treated at 350°C for 8 h, LiH phase disappears. On the other hand, new diffraction peaks assigned to Li_2C_2 appear as shown in Fig. 2 (b) although the peaks are quite small. By the 1st rehydrogenation at 350°C for 8 h under H_2 pressure of 3 MPa, the Li_2C_2 phase disappears, and then, the LiH phase is recovered as shown in Fig. 2 (a). With the re/dehydrogenation treatments after the 3rd cycle, it is clearly found that the peaks assigned to LiH remain in the dehydrogenating sample. The diffraction peaks corresponding to Li_2C_2 are grown by the 2nd dehydrogenation treatment, however they gradually decrease from the 3rd cycle. These results indicate that the formation of Li_2C_2 due to the interaction between the polarized C−H groups in $C^{nano}H_x$ and LiH decreases from the 3rd cycle. The phenomenon is quite consistent with the decrease in the hydrogen desorption amount after the 3rd cycle obtained by TG.

The local chemical bonding states of the as-synthesized, 1st dehydrogenated, and 1st rehydrogenated composites were investigated by the neutron diffraction to understand the variation of the nano-structural graphite. The structure factors (S(*Q*)) of the $C^{nano}D_x$−LiD composite at each state are shown in Fig. 3, where the S(*Q*) of host graphite and LiD measured as reference are also included in the figure (Miyaoka et al., 2008).

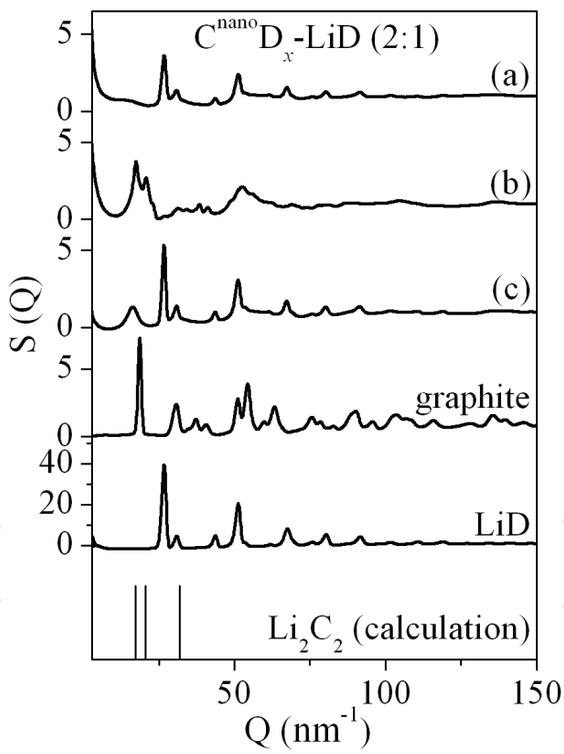

Fig. 3. Structure factors (S(*Q*)) of (a) the as-synthesized, (b) the 1st dehydrogenated, (c) the 1st rehydrogenated $C^{nano}D_x$-LiD composite. The lower spectra are S(*Q*) of host graphite, LiD and main peaks of Li_2C_2 calculated form database (PDF #21-0484) as reference.

As shown in Fig. 3 (a), no peaks corresponding to graphite are observed in the spectrum of the as−synthesized composite although some observed peaks are assigned to LiD by comparing with the reference. Additionally, a large scattering intensity is observed in the

small angle scattering region below 5.0 nm^{-1} in S(Q). This result indicates that the graphite in the composite possesses the disordered states such as nano−structure or amorphous structure. Fig. 3 (b) shows S(Q) of the dehydrogenated composite. Moreover, main peaks of Li_2C_2 calculated from powder X−ray diffraction file of L_2C_2 (PDF #21−0484) in database are also shown in Fig. 3, where intensity of each peak is assumed to be unity. The peaks corresponding to LiD completely disappear after the dehydrogenation. On the other hand, new peaks are observed, in which these are not consistent with the peaks corresponding to graphite shown as a reference. Among them, main peaks observed in S(Q) are consistent with the peaks calculated from database of Li_2C_2. Therefore, it is considered that the peaks observed after the dehydrogenation would be assigned to Li_2C_2. As shown in Fig. 3 (c), it is observed that the peaks corresponding to LiD are recovered after rehydrogenation. Moreover, broad peak appears around 1.6 nm^{-1} in S(Q), which would be assigned to the graphite (002), where it is noticed that the position of this peak is slightly shifted to lower Q compared with that of graphite shown as a reference. It is expected that this peak shift is induced by expansion of the graphite layers due to grain size of nano−meter order. In addition to this result, the intensity in the small angle scattering region decreases compared with those of the as−synthesized and dehydrogenated composite. From these results, it is suggested that a small part of nano−structural graphite would be ordered by rehydrogenating treatment.

The Radial distribution function RDF(r) obtained from S(Q) of the composites at each stage are shown in Fig. 4 (Miyaoka et al., 2008).

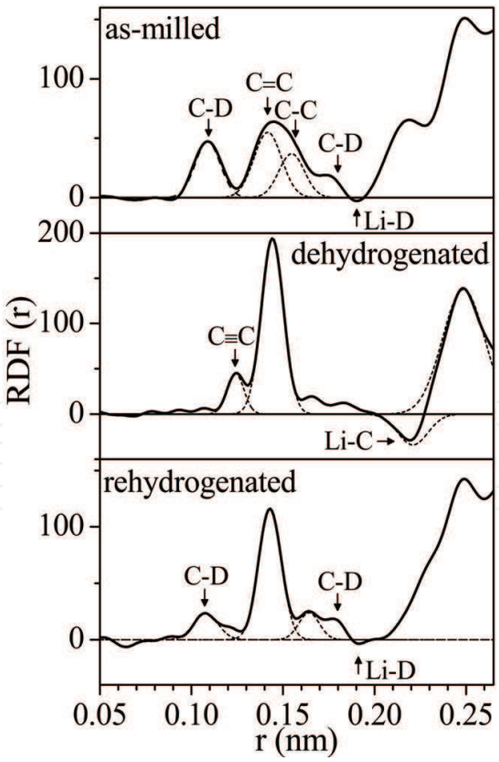

Fig. 4. Radial distribution function RDF(r) of the as-synthesized, dehydrogenated, and rehydrogenated $C^{nano}D_x$-LiD composites. Dashed lines represent the fits using Gaussian distribution functions.

For the peaks observed within 0.25 nm, the correlations between atoms are estimated by fitting used Gaussian distribution functions. Furthermore, some C−H groups, which are −CH, $-CH_2$ and $-CH_3$, are shown as models of hydrogen chemisorbed states in Fig. 5, where these models are built by geometric expectations and the previous studies (Miyaoka et al., 2008). In this RDF(*r*) of the as-milled composite, two kinds of peaks related to C−C correlation are observed at about 0.14 and 0.15 nm. The peak around 0.14 nm would originate in the bonding of sp^2−hybridized carbon atoms (C=C) in hexatomic ring of graphite structure. With respect to another peak corresponding to the C−C correlation, the bond length of 0.15 nm is close to that of sp^3−hybridized carbon atoms (C−C) in crystalline diamond. Thus, it is expected that the 4−fold bonding is generated due to the destruction of graphite structure by using ball−milling as shown in Fig. 5 (d) and (e). It is also possible that some kinds of chained C−H groups with the C−C sp^3−bonding may exist at the edges in the nano−structural graphite. Furthermore, the peaks corresponding to two kinds of the C−D correlations are observed at about 0.11 and 0.18 nm, respectively. The C−D correlation observed around 0.11 nm is ascribed to the covalent bonds, (Fukunaga et al., 2004) suggesting that hydrogen atoms are chemisorbed at dangling bonds such as the edges or as the defects in graphene sheets produced by ball−milling as models shown in Fig. 5. It is considered that the C−D peak around 0.18 nm is assigned to the correlation between hydrogen atoms of the C−D groups at the graphene edges and second neighbor carbon atoms (C^{2nd}−D). For these models of the C−H group, the C^{2nd}−H bond length is estimated by a geometrical calculation as follows. The C^{2nd}−H bond length in case of the covalent bond at zigzag edges in ab−plane as model (a) is estimated to be about 0.22 nm, which is longer than 0.18 nm. On the other hand, it is possible that the C^{2nd}−H bond length of other models is estimated to be around 0.18 nm if the atoms form a suitable C−C−H bond angle. The bond length of 0.18 nm might be realized in a situation when the hydrogen atom in the model (a), (b), and (c) exists at out of ab−plane, where the C−C−H bond angle should be around 91 °. In addition to above C−C and C−D correlations, it is noticed that the negative correlation is revealed at about 0.19 nm. In fact, this peak is not clear because the negative peak overlaps with the positive correlation around 0.18 nm, so that it is quite difficult to perform the fitting by Gaussian distribution functions for both peaks. Here, it is clarified from RDF(*r*) obtained by neutron diffraction for LiD itself that the Li−D correlation is revealed as negative peak because a coherent scattering length of Li atom is only negative value among those of the atoms included in this composite. Furthermore, the result of the XRD measurements and S(*Q*) of the $C^{nano}D_x$−LiD composites demonstrated the existence of LiD. From these experimental facts, the negative correlation is assigned to the Li−D bond.

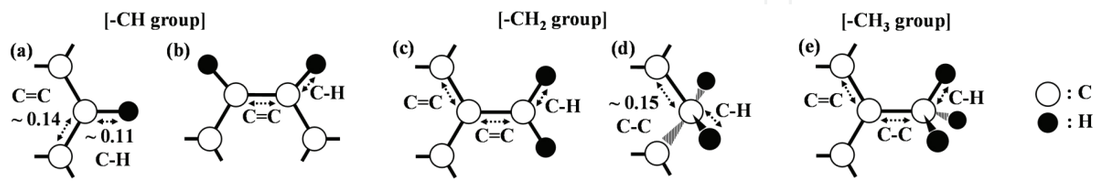

Fig. 5. Models of hydrogen chemisorbed state as -CH, $-CH_2$ and $-CH_3$ groups in the $C^{nano}H_x$-LiH composite; (a) -CH group at zigzag edges and (b) arm-chair edges, (c) $-CH_2$ group with sp^2-hybridyzed carbon (C=C) and (d) sp^3-hybridyzed carbon (C-C), (e) $-CH_3$ group, where shown unit of length is nm.

In the RDF(r) of the dehydrogenated $C^{nano}D_x$−LiD composite, three kinds of characteristic peaks are revealed at about 0.12, 0.14 and 0.22 nm. The peak around 0.14 nm is assigned to the C=C correlation of sp^2−bonding in nano−structural graphite, which is sharper than that of as−synthesized composite. The positive peak around 0.12 nm and the negative peak around 0.22 nm are ascribed to the C−C and C−Li correlation in Li_2C_2, respectively. The crystal structure of Li_2C_2 have been investigated and reported before. (Juza et al., 1967, Ruschewitz & Pottgen, 1999) Among those studies, Ruschewitz *et al*. reported on the crystal structure Li_2C_2 obtained by X−ray diffraction measurements. (Ruschewitz & Pottgen, 1999) In that paper, it is determined that the bond length of the C−C correlation in Li_2C_2 is about 0.123 nm. This C−C bond would be the typical C−C triple bond (C≡C) of sp−hybridization, where this bond length is close to that of 0.120 nm in acetylene. Thus, the C−C correlation around 0.12 nm is assigned to the C−C triple bond in Li_2C_2. The obvious negative peak around 0.22 nm should be ascribed in a correlation related to Li atom. By comparing with the RDF(r) of the as−synthesized composite, this bond length is longer than that of 0.19 nm in case of the Li−D correlation. It is confirmed from XRD pattern and S(Q) that the LiD phase disappeared after dehydrogenation. From these experimental facts, it can be explained that the origin of the peak around 0.22 nm is caused by the C−Li correlation in Li_2C_2. In the case of the rehydrogenated composite, the peaks assigned to Li_2C_2 disappear and the Li−D correlation assigned to LiD phase is recovered at about 0.19 nm, where this phenomenon has been clarified by the XRD measurement already. The peak ascribed to the C=C sp^2−bonding is also observed around 0.14 nm. On the other hand, the peak at 0.15 nm of as−synthesized composite is not revealed in the RDF(r) profile of the rehydrogenated composite. Considering these result, it is expected that the amount of sp^3−hybridyzed carbon atoms decrease due to the structural order by the hydrogen desorption and absorption treatments, where this result is consistent with the behavior in the small angle scattering region in S(Q). It is noticed that the peaks corresponding to the C−D correlation are obviously recovered around 0.11 and 0.18 nm. Therefore, it is considered that the only hydrogen desorption from the rehydrogenated composite is realized by the interaction between the polarized C−H bonding at the dangling bonds of nano−structural graphite and LiH. The intensity of the peak around 0.11 nm is slightly weak, in comparison to that of the as−synthesized composite, indicating that the amount of chemisorbed hydrogen at the dangling bonds is smaller than that in the as−synthesized composite. In addition, new peak is observed at about 0.16 nm, which is longer than that of the C−C bonds of ~0.15 nm or shorter than that of C^{2nd}−H bond of ~0.18 nm. Thus, it seems likely that the origin of this peak might be a new C−D correlation, which is different from the C^{2nd}−D correlation revealed around 0.18 nm, as a one of the possibilities. From the above results of the neutron diffraction measurements, it is clarified that not only Li but also nano−structural carbon (C^{nano}) in this composite can be recharged with hydrogen by the rehydrogenating treatment at 350 °C under 3 MPa of hydrogen pressure.

In order to understand the hydrogen absorption process in further detail, the gases remaining in the reactor, are examined by GC after each rehydrogenation. The gas chromatograms for the composites are shown in Fig. 6 (a), and the results of GC for H_2 and CH_4 gases are appended in Fig. 6 (b) as references (Miyaoka et al., 2009). All the chromatograms of the composites show two peaks at different retention times. The respective peaks are assigned to H_2 and CH_4 because the positions of peaks are quite consistent with those of the reference. The results

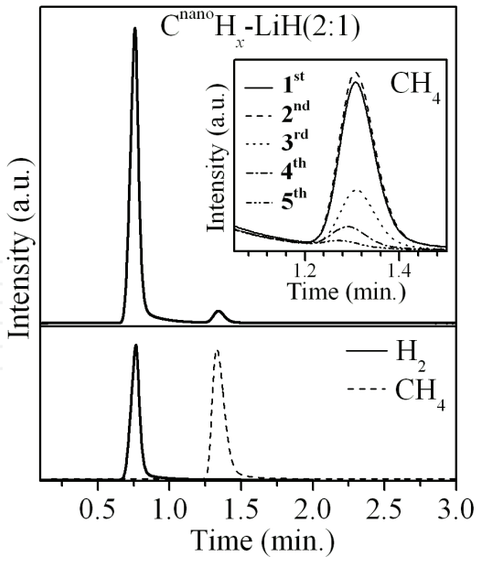

Fig. 6. (a) The chromatograms of the gases remaining in the reactor after each rehydrogenation of the $C^{nano}H_x$-LiH composite by heat treatment at 350°C for 8 h under 3 MPa of hydrogen, and the second peaks observed after each rehydrogenation are shown in inset, in which the peak intensity is normalized by the intensity of first peak. (b) The chromatogram of H_2 and CH_4 itself as reference.

indicate that the hydrocarbons, mainly CH_4, are desorbed with decomposition of Li_2C_2 by recharging the composite with the hydrogen, where a quite small amount of ethane C_2H_6 is also observed in the GC. As shown in the inset of Fig. 6 (a), the normalized intensity of the peak ascribed to CH_4 is gradually weakened by the 3rd rehydrogenation, in which the normalization of the peaks is carried out by using the intensity of H_2.

Fig. 7 shows the amount of carbon lost as hydrocarbon during each rehydrogenating treatment as a function of the number of hydrogen ab/desorption cycles, assuming that the desorbed gas is only CH_4 (Miyaoka et al., 2009).

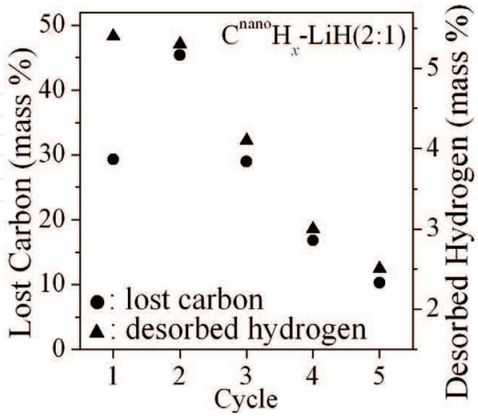

Fig. 7. Amounts of the carbon lost during each rehydrogenation of the $C^{nano}H_x$-LiH composite and the hydrogen desorbed from the each rehydrogenated composite as a function of the hydrogen ab/desorption cycle, which are estimated by the results from GC and TG, respectively.

The amount of carbon in CH_4 and H_2 are estimated respectively by the GC and TG. At the 1st cycle, about 29.0 mass % of the carbon atoms is desorbed as CH_4 and 5.0 mass % of H_2 is desorbed from the composite. The amount of lost carbon is reached up to 45.4 mass % at the 2nd hydrogen recharge, and gradually decreases with the hydrogenating treatment from the 3rd cycle. The decrease in the hydrogen desorption amount is also started from the 3rd cycle. The variation of the amount of lost carbon and desorbed hydrogen by the hydrogenation and dehydrogenation cycles is quite consistent with each other. Therefore, the results of GC indicate that the hydrogen absorption and desorption properties of the composite are strongly related to the hydrocarbon desorption during the hydrogen recharging process.
From the above experimental facts and the following four assumptions,

1. the quite small amount of hydrocarbons desorption from the as−synthesized composite can be ignored (Fig. 1),
2. the hydrogenated state of the ball−milled graphite in the composite after rehydrogenation is defined as the $C^{nano}H_y$ because the rehydrogenated state of the composite is different from that of $C^{nano}H_x$ in the as−synthesized composite , and the $H/C = y$ is not changed with the cycled treatments,
3. the half of the carbons in the Li_2C_2 is desorbed as CH_4 gas with recharging hydrogen, and
4. H_2 or CH_4 desorbed by each treatment is removed from the system,

it is expected that the hydrogen absorption and desorption reaction in the Li−C−H system with the cycles of hydrogenation and dehydrogenation treatments is expressed as follows (Miyaoka et al., 2009):

Initial desorption: $$2C^{nano}H_x + LiH \rightarrow C^{nano} + \frac{1}{2}Li_2C_2 + \left(\frac{4x+2}{4}\right)H_2 \uparrow \quad (1)$$

1st cycle: (abs.) $$C^{nano} + \frac{1}{2}Li_2C_2 + \left(\frac{3y+6}{4}\right)H_2 \rightarrow \frac{3}{2}C^{nano}H_y + \frac{1}{2}CH_4 \uparrow + LiH \quad (2)$$

(des.) $$\frac{3}{2}C^{nano}H_y + LiH \rightarrow \frac{1}{2}C^{nano} + \frac{1}{2}Li_2C_2 + \left(\frac{3y+2}{4}\right)H_2 \uparrow \quad (3)$$

2nd cycle: (abs.) $$\frac{1}{2}C^{nano} + \frac{1}{2}Li_2C_2 + \left(\frac{2y+6}{4}\right)H_2 \rightarrow C^{nano}H_y + \frac{1}{2}CH_4 \uparrow + LiH \quad (4)$$

(des.) $$C^{nano}H_y + LiH \rightarrow \frac{1}{2}Li_2C_2 + \left(\frac{2y+2}{4}\right)H_2 \uparrow \quad (5)$$

3rd cycle: (abs.) $$\frac{1}{2}Li_2C_2 + \left(\frac{y+6}{4}\right)H_2 \rightarrow \frac{1}{2}\left(C^{nano}H_y + CH_4 \uparrow\right) + LiH \quad (6)$$

(des.) $$\frac{1}{2}C^{nano}H_y + LiH \rightarrow \frac{1}{4}Li_2C_2 + \left(\frac{y+1}{4}\right)H_2 \uparrow + \frac{1}{2}LiH \quad (7)$$

4th cycle: (abs.) $$\frac{1}{4}Li_2C_2 + \frac{1}{2}LiH + \left(\frac{y+6}{8}\right)H_2 \rightarrow \frac{1}{4}\left(C^{nano}H_y + CH_4 \uparrow\right) + LiH \quad (8)$$

$$\text{(des.)} \quad \frac{1}{4}\mathrm{C^{nano}H}_y + \mathrm{LiH} \rightarrow \frac{1}{8}\mathrm{Li_2C_2} + \left(\frac{y+1}{8}\right)\mathrm{H_2}\uparrow + \frac{3}{4}\mathrm{LiH} \tag{9}$$

$$\text{5th cycle: (abs.)} \quad \frac{1}{8}\mathrm{Li_2C_2} + \frac{3}{4}\mathrm{LiH} + \left(\frac{y+6}{16}\right)\mathrm{H_2} \rightarrow \frac{1}{8}\left(\mathrm{C^{nano}H}_y + \mathrm{CH_4}\uparrow\right) + \mathrm{LiH} \tag{10}$$

$$\text{(des.)} \quad \frac{1}{8}\mathrm{C^{nano}H}_y + \mathrm{LiH} \rightarrow \frac{1}{16}\mathrm{Li_2C_2} + \left(\frac{y+1}{16}\right)\mathrm{H_2}\uparrow + \frac{7}{8}\mathrm{LiH}\,. \tag{11}$$

In this reaction model, the non−reacted LiH remains from the 3rd cycle. The hydrogen ab/desorption reactions of the Li−C−H system from the 3rd cycles can be described as following equations (n = 1, 2, 3…),

$$n^{\text{th}}\text{ cycle: (abs.)} \quad \frac{1}{2^n}\mathrm{Li_2C_2} + \left(\frac{2^{n-1}-1}{2^{n-1}}\right)\mathrm{LiH} + \left(\frac{y+6}{2^{n+1}}\right)\mathrm{H_2} \rightarrow \frac{1}{2^n}\left(\mathrm{C^{nano}H}_y + \mathrm{CH_4}\uparrow\right) + \mathrm{LiH} \tag{12}$$

$$\text{(des.)} \quad \frac{1}{2^n}\mathrm{C^{nano}H}_y + \mathrm{LiH} \rightarrow \frac{1}{2^{n+1}}\mathrm{Li_2C_2} + \left(\frac{y+1}{2^{n+1}}\right)\mathrm{H_2}\uparrow + \left(\frac{2^n-1}{2^n}\right)\mathrm{LiH}\,. \tag{13}$$

Therefore, it is considered that the model of hydrogen absorption/desorption reactions of the Li−C−H system expressed by the above equations would describe the experimental results obtained in this work.

3.2 Hydrogen desorption properties of the $C^{nano}H_xMH$(M=Na, Mg, and Ca) composite

Fig. 8 shows the results obtained by (a) TDMS, (b) TG-DSC, and (c) XRD measurements of the $C^{nano}H_x$−NaH composite, where the intensity of hydrocarbons is enlarged ten times (Miyaoka et al., 2007). As shown in inset, the TDMS profile indicates that the milled NaH needs 320 °C to release hydrogen gas. On the other hand, the composite exhibits a broad sub−peak at slightly lower temperature than the temperature corresponding to a main peak for hydrogen desorption, where these peaks are located around 260 and 300 °C, respectively. It should be noted that their hydrogen desorption temperatures are lower than those of constituent components. Accompanied by the lower hydrogen desorption corresponding to 260 °C, it is noticed that quite small amount of hydrocarbons are desorbed from the composite as well. However, the hydrocarbons desorption is immediately suppressed with further increasing temperature after showing a broad peak around 260 °C. Fig. 8 (b) shows the TG and DSC profiles for the $C^{nano}H_x$−NaH composite. The DSC spectrum indicates that both the reactions at the sub and the main peaks in the TDMS spectrum at 260 and 300 °C are endothermic, suggesting that the reactions are rechargeable. Additionally, the weight loss of the composite was estimated to be ~5 mass% as shown in the TG profile, though the weight loss due to the decomposition of lone NaH in the composite is theoretically estimated to ~2 mass%. This suggests that hydrogen in $C^{nano}H_x$ is also synchronously desorbed at the same temperatures as the hydrogen desorption. Fig. 8 (c) shows the XRD pattern for the $C^{nano}H_x$ and NaH composite before and after the thermal gas−desorption examination. Mainly, the peaks corresponding to the NaH phase are observed because the $C^{nano}H_x$ phase itself does not show any diffraction peaks (Isobe et al., 2004). The XRD pattern

of the composite after increasing temperature up to 350 °C indicates only the appearance of metallic Na phase. This fact shows that the hydrogen desorption is at least caused by the decomposition of NaH. Moreover, since hydrogen in the $C^{nano}H_x$ phase is also destabilized by making composite with NaH, a composite of Na and C^{nano} is supposed to be formed by dehydrogenation. However, the metallic Na phase is clearly observed, indicating that not only the nano−composite phase between Na and C^{nano} but also the disproportionating phases are formed after dehydrogenation. This behavior seems to be originated in a quite low melting point of Na (below 100 °C).

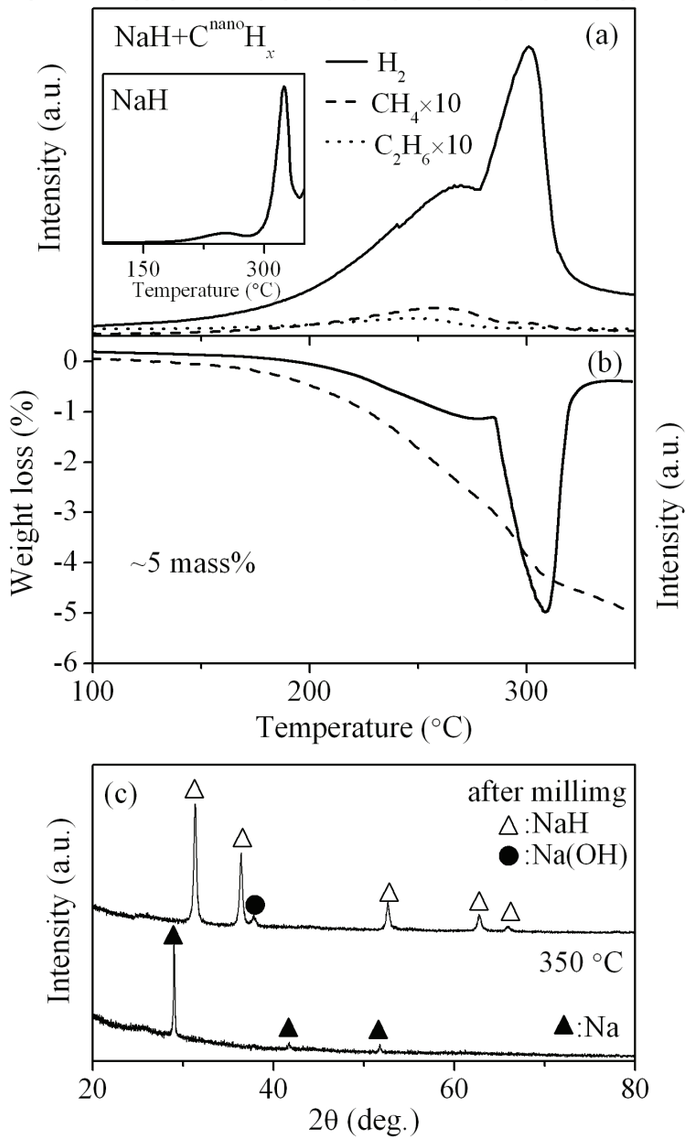

Fig. 8. (a) TDMS profiles of hydrogen and hydrocarbons from the $C^{nano}H_x$–NaH composite, and the inset shows TDMS profile of the milled NaH. (b) TG (dashed line) and DSC (solid line) spectra of the composite. (c) The XRD patterns after milling and after heating up to 350 °C of the composite.

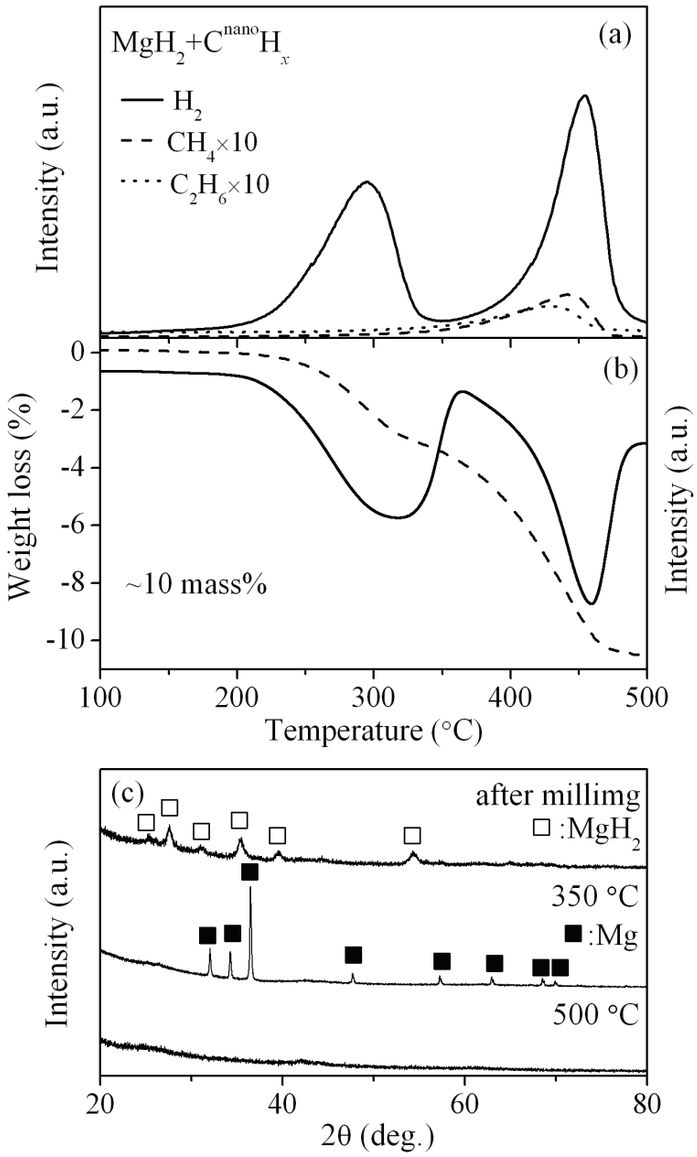

Fig. 9. (a) TDMS profiles of hydrogen and hydrocarbons from the $C^{nano}H_x$–MgH_2 composite, where the intensity of hydrocarbons are enlarged ten times. (b) TG (dashed line) and DSC (solid line) spectra of the composite. (c) The XRD patterns after milling, after heating up to 350 °C and 500 °C of the composite.

The results of thermal and structural analyses for the $C^{nano}H_x$–MgH_2 composite are shown Fig. 9 (Miyaoka et al., 2007). This composite desorbs hydrogen with two peaks. The first and second hydrogen desorption peaks were located around 300 and 450 °C, respectively. The first hydrogen desorption temperature was lower than ~350 °C, which seems to correspond to the typical decomposition temperature of pure MgH_2 milled for 2 h (Hanada et al., 2005, Hanada et al., 2005). Actually, the metallic Mg phase appears in the XRD pattern after desorbing hydrogen at 350 °C as shown in Fig. 9 (c). Moreover, the TG profile of the composite as shown in Fig. 9 (b) reveals ~3 mass% weight loss until 350°C, where the weight

loss is consistent with the calculated value of hydrogen desorption due to decomposition of pure MgH_2 in the composite, indicating that only the decomposition of MgH_2 occurs until 350 °C. Therefore, the above results suggest that the MgH_2 solid phase does not such strongly interact with the $C^{nano}H_x$ product. On the other hand, when the temperature was increased up to 500 °C corresponding to a higher temperature than a second hydrogen desorption peak one, no evident peak appears in the XRD pattern, indicating that a nano−structural cluster composed of a metallic Mg and nano−structural carbon is generated at 500 °C after desorbing hydrogen by an interaction between Mg and $C^{nano}H_x$. Actually, the amount of the corresponding hydrocarbons is quite small compared with that from $C^{nano}H_x$ itself. This result indicates that hydrogen is desorbed instead of hydrocarbon due to destabilization of hydrocarbons group in the $C^{nano}H_x$ product by an interaction with the Mg solid phase. The total amounts of weight loss reach up to ~10 mass% with increasing temperature up to 500 °C in the TG profile. The composite is also expected to be rehydrogenated because two endothermic peaks clearly appear at 300 and 450 °C in the DSC spectrum, respectively.

Fig. 10 shows (a) TDMS, (b) TG-DSC, and (c) XRD results of the $C^{nano}H_x$−CaH_2 composite, where the intensity of hydrocarbons are enlarged ten times (Miyaoka et al., 2007). As is shown in Fig. 10 (a), the hydrogen desorption spectrum for the $C^{nano}H_x$ and CaH_2 composite shows a two−peak structure in the temperature range from 300 to 500 °C, where the CaH_2 hydride itself could not be decomposed by heating up to 500 °C. Furthermore, the suppression of hydrocarbons is found in the TDMS profile by making composite of $C^{nano}H_x$ with CaH_2, indicating that the C−H bonding in the hydrocarbon groups in the $C^{nano}H_x$ product is weakened by an interaction between CaH_2 and $C^{nano}H_x$. Then, the composite exhibits a weight loss of ~8 mass% in the TG profile by heating up to 500 °C as shown in Fig. 10 (b), where the weight loss caused by decomposition of lone CaH_2 is theoretically estimated to ~2 mass% in the composite. This suggests that hydrogen in the $C^{nano}H_x$ product is synchronously desorbed at the same temperature as CaH_2 desorbs hydrogen as well. Thermal analysis due to the DSC measurement indicates that the hydrogen desorption reaction of the composite is weakly endothermic as shown in Fig. 10 (b). This result suggests that the rehydrogenation reaction is expected to occur in the $C^{nano}H_x$ and CaH_2 composite similar to the other metal−C−H materials. Fig. 10 (c) shows the XRD patterns on the composite. After increasing temperature up to 500 °C, the intensity corresponding to CaH_2 in the XRD pattern is significantly suppressed compared with that before dehydrogenation. Furthermore, the XRD profile of the composite exhibits no existence of Ca or CaC_2 after dehydrogenation at 500 °C. Therefore, it is suggested that a nano−structural cluster composed of C^{nano} and Ca is formed in the composite after the dehydrogenation.

4. Conclusion

The hydrogen desorption of $C^{nano}H_x$ is lowed to 350 °C by synthesizing the composite with LiH, indicating that the C-H bonds in $C^{nano}H_x$ is destabilized by the interaction with LiH. Such destabilization of the C-H bonds is also clarified in the case of the composite of $C^{nano}H_x$ and other alkali(-earth) metal hydride. The $C^{nano}H_x$−LiH composite rechargeably store 5.0 mass % of hydrogen until the 2nd cycle. The hydrogenated state of this composite is the C-H bonds at the graphene edges and defects in the nano-structural graphite and LiH, and its

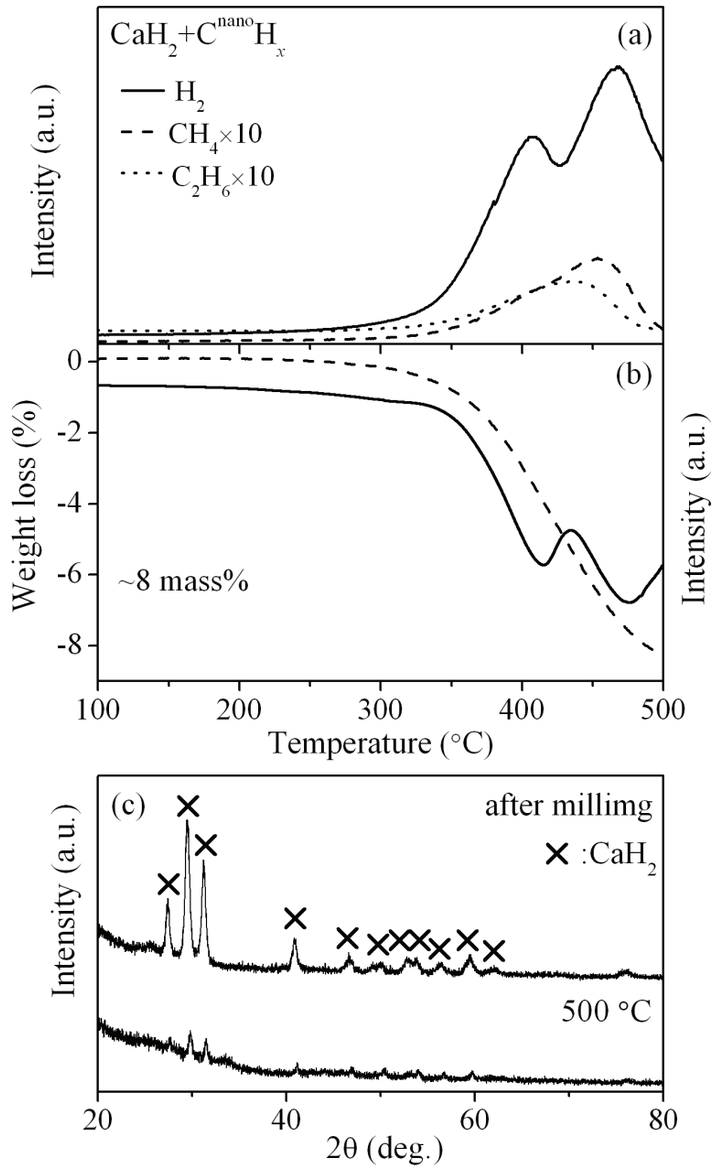

Fig. 10. (a) TDMS profiles of hydrogen and hydrocarbons from the $C^{nano}H_x$–CaH_2 composite. (b) TG (dashed line) and DSC (solid line) spectra of the composite. (c) The XRD patterns after milling, after heating up to 500 °C of the composite.

dehydrogenated state is Li_2C_2 and nano-structural graphite without the C-H bonds. The hydrogen desorption amount gradually decreases from the 3rd cycle. In the hydrogen absorption process, considerable amount of hydrocarbon was generated, indicating that the carbon atoms in the composite are lost with each hydrogen recharging process. Therefore, it is considered that the decrease in the rechargeable hydrogen amount is caused by desorbing hydrocarbons with the decomposition of Li_2C_2 under rehydrogenation process, in other words, the amount of the hydrogen desorption reaction between the polarized groups composed of the C−H bonds and LiH are gradually reduced due to decrease in the C−H groups by the loss of the carbon atoms with the rehydrogenation.

The Li−C−H system would be recognized as one of attractive systems for hydrogen storage. However, the hydrocarbon desorption during hydrogen recharging process is essentially a problem on this system, because it reduces the hydrogen absorption amount. For practical use as hydrogen storage system, an improvement, e.g. usage of a catalyst or scaffold, is needed to prevent the hydrocarbon desorption during the hydrogenation.

5. References

Akiba, E. (1999). Hydrogen-absorbing alloys. *Curr. Opin. Solid State Mater. Sci.*, 4, 3, 267-272, 1359-0286.

Chen, D. M.; Ichikawa, T.; Fujii, H.; Ogita, N.; Udagawa, M.; Kitano, Y. & Tanabe, E. (2003). Unusual hydrogen absorption properties in graphite mechanically milled under various hydrogen pressures up to 6 MPa. *J. Alloys Compd.*, 354, 1-2, L5-L9, 0925-8388.

Dillon, A. C.; Jones, K. M.; Bekkedahl, T. A.; Kiang, C. H.; Bethune, D. S. & Heben, M. J. (1997). Storage of hydrogen in single-walled carbon nanotubes. *Nature*, 386, 6623, 377-379, 0028-0836.

Fukunaga, T.; Itoh, K.; Orimo, S. & Aoki, K. (2004). Structural observation of nano-structured and amorphous hydrogen storage materials by neutron diffraction. *Mat. Sci. Eng. B-Solid State Mat. Adv. Technol.*, 108, 1-2, 105-113, 0921-5107.

Grochala, W. & Edwards, P. P. (2004). Thermal decomposition of the non-interstitial hydrides for the storage and production of hydrogen. *Chem. Rev.*, 104, 3, 1283-1315, 0009-2665.

Hanada, N.; Ichikawa, I. & Fujii, H. (2005). Catalytic effect of Ni nano-particle and Nb oxide on H-desorption properties in MgH_2 prepared by ball milling. *J. Alloys Compd.*, 404-406, 716-719, 0925-8388.

Hanada, N.; Ichikawa, T. & Fujii, H. (2005). Catalytic effect of nanoparticle 3d-transition metals on hydrogen storage properties in magnesium hydride MgH_2 prepared by mechanical milling. *J. Phys. Chem. B*, 109, 15, 7188-7194, 1520-6106.

Ichikawa, T.; Chen, D. M.; Isobe, S.; Gomibuchi, E. & Fujii, H. (2004). Hydrogen storage properties on mechanically milled graphite. *Mat. Sci. Eng. B-Solid State Mat. Adv. Technol.*, 108, 1-2, 138-142, 0921-5107.

Ichikawa, T.; Fujii, H.; Isobe, S. & Nabeta, K. (2005). Rechargeable hydrogen storage in nanostructured mixtures of hydrogenated carbon and lithium hydride. *Appl. Phys. Lett.*, 86, 24, 241914,

Ichikawa, T.; Hanada, N.; Isobe, S.; Leng, H. Y. & Fujii, H. (2004). Mechanism of novel reaction from $LiNH_2$ and LiH to Li_2NH and H_2 as a promising hydrogen storage system. *J. Phys. Chem. B*, 108, 23, 7887-7892, 1520-6106.

Ichikawa, T.; Isobe, S. & Fujii, H. (2005). Hydrogen desorption properties of lithium-carbon-hydrogen system. *Mater. Trans.*, 46, 8, 1757-1759, 1345-9678.

Isobe, S.; Ichikawa, T.; Gottwald, J. I.; Gomibuchi, E. & Fujii, H. (2004). Catalytic effect of 3d transition metals on hydrogen storage properties in mechanically milled graphite. *J. Phys. Chem. Solids*, 65, 2-3, 535-539, 0022-3697.

Itoh, K.; Miyahara, Y.; Orimo, S.; Fujii, H.; Kamiyama, T. & Fukunaga, T. (2003). The local structure of hydrogen storage nanocrystalline graphite by neutron scattering. *J. Alloys Compd.*, 356, 608-611, 0925-8388.

Juza, R.; Wehle, V. & Schuster, H. U. (1967). Zur Kenntnis Des Lithiumacetylids. *Z. Anorg. Allg. Chem.*, 352, 5-6, 252, 0044-2313.

Majer, G.; Stanik, E. & Orimo, S. (2003). NMR studies of hydrogen motion in nanostructured hydrogen-graphite systems. *J. Alloys Compd.*, 356, 617-621, 0925-8388.

Miyaoka, H.; Ichikawa, T. & Fujii, H. (2007). Thermodynamic and structural properties of ball-milled mixtures composed of nano-structural graphite and alkali(-earth) metal hydride. *J. Alloys Compd.*, 432, 1-2, 303-307, 0925-8388.

Miyaoka, H.; Ichikawa, T.; Fujii, T.; Ishida, W.; Isobe, S.; Fujii, H. & Kojima, Y. (2010). Anomalous hydrogen absorption on non-stoichiometric iron-carbon compound. *J. Alloys Compd.*, 507, 2, 547-550, 0925-8388.

Miyaoka, H.; Ichikawa, T. & Kojima, Y. (2009). The reaction process of hydrogen absorption and desorption on the nanocomposite of hydrogenated graphite and lithium hydride. *Nanotechnology*, 20, 20, 204021, 0957-4484.

Miyaoka, H.; Itoh, K.; Fukunaga, T.; Ichikawa, T.; Kojima, Y. & Fuji, H. (2008). Characterization of hydrogen absorption/desorption states on lithium-carbon-hydrogen system by neutron diffraction. *J. Appl. Phys.*, 104, 5, 053511-053517,

Ogita, N.; Yamamoto, K.; Hayashi, C.; Matsushima, T.; Orimo, S.; Ichikawa, T.; Fujii, H. & Udagawa, M. (2004). Raman scattering and infrared absorption investigation of hydrogen configuration state in mechanically milled graphite under H_2 gas atmosphere. *J. Phys. Soc. Jpn.*, 73, 3, 553-555, 0031-9015.

Orimo, S.; Majer, G.; Fukunaga, T.; Züttel, A.; Schlapbach, L. & Fujii, H. (1999). Hydrogen in the mechanically prepared nanostructured graphite. *Appl. Phys. Lett.*, 75, 20, 3093-3095, 0003-6951.

Orimo, S.; Matsushima, T.; Fujii, H.; Fukunaga, T. & Majer, G. (2001). Hydrogen desorption property of mechanically prepared nanostructured graphite. *J. Appl. Phys.*, 90, 3, 1545-1549, 0021-8979.

Orimo, S. I.; Nakamori, Y.; Eliseo, J. R.; Zuttel, A. & Jensen, C. M. (2007). Complex hydrides for hydrogen storage. *Chem. Rev.*, 107, 10, 4111-4132, 0009-2665.

Ruschewitz, U. & Pottgen, R. (1999). Structural phase transition in Li_2C_2. *Z. Anorg. Allg. Chem.*, 625, 10, 1599-1603, 0044-2313.

Sandrock, G. (1999). A panoramic overview of hydrogen storage alloys from a gas reaction point of view. *J. Alloys Compd.*, 295, 877-888, 0925-8388.

Schüth, F.; Bogdanović, B. & Felderhoff, M. (2004). Light metal hydrides and complex hydrides for hydrogen storage. *Chem. Commun.*, , 20, 2243-2248,

Schlapbach, L. & Züttel, A. (2001). Hydrogen-storage materials for mobile applications. *Nature*, 414, 6861, 353-358, 0028-0836.

Smith, C. I.; Miyaoka, H.; Ichikawa, T.; Jones, M. O.; Harmer, J.; Ishida, W.; Edwards, P. P.; Kojima, Y. & Fuji, H. (2009). Electron Spin Resonance Investigation of Hydrogen Absorption in Ball-Milled Graphite. *J. Phys. Chem. C*, 113, 14, 5409-5416, 1932-7447.

Stanik, E.; Majer, G.; Orimo, S.; Ichikawa, T. & Fujii, H. (2005). Nuclear-magnetic-resonance measurements of the hydrogen dynamics in nanocrystalline graphite. *J. Appl. Phys.*, 98, 4, 044302, 0021-8979.

Züttel, A. (2004). Hydrogen storage methods. *Naturwissenschaften*, 91, 4, 157-172, 0028-1042.

Züttel, A. (2007). Hydrogen storage and distribution systems. *Mitig. Adapt. Strat. Glob. Change*, 12, 3, 343-365

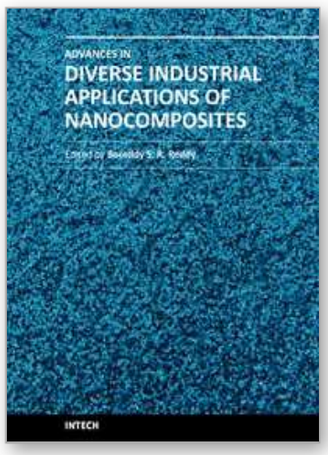

Advances in Diverse Industrial Applications of Nanocomposites
Edited by Dr. Boreddy Reddy

ISBN 978-953-307-202-9
Hard cover, 550 pages
Publisher InTech
Published online 22, March, 2011
Published in print edition March, 2011

Nanocomposites are attractive to researchers both from practical and theoretical point of view because of combination of special properties. Many efforts have been made in the last two decades using novel nanotechnology and nanoscience knowledge in order to get nanomaterials with determined functionality. This book focuses on polymer nanocomposites and their possible divergent applications. There has been enormous interest in the commercialization of nanocomposites for a variety of applications, and a number of these applications can already be found in industry. This book comprehensively deals with the divergent applications of nanocomposites comprising of 22 chapters.

How to reference
In order to correctly reference this scholarly work, feel free to copy and paste the following:

Takayuki Ichikawa, Hiroki Miyaoka and Yoshitsugu Kojima (2011). Hydrogen Storage Properties of Hydrogenated Graphite and Lithium Hydride Nanocomposite, Advances in Diverse Industrial Applications of Nanocomposites, Dr. Boreddy Reddy (Ed.), ISBN: 978-953-307-202-9, InTech, Available from: http://www.intechopen.com/books/advances-in-diverse-industrial-applications-of-nanocomposites/hydrogen-storage-properties-of-hydrogenated-graphite-and-lithium-hydride-nanocomposite

INTECH
open science | open minds

InTech Europe
University Campus STeP Ri
Slavka Krautzeka 83/A
51000 Rijeka, Croatia
Phone: +385 (51) 770 447
Fax: +385 (51) 686 166
www.intechopen.com

InTech China
Unit 405, Office Block, Hotel Equatorial Shanghai
No.65, Yan An Road (West), Shanghai, 200040, China
中国上海市延安西路65号上海国际贵都大饭店办公楼405单元
Phone: +86-21-62489820
Fax: +86-21-62489821

IntechOpen